Обзор ArXiv/astro-ph, 24-30 марта 2026

От Сильченко О.К.

ArXiv: 2603.23981

A Long Stellar Stream in M83: Possible Connection Between XUV Disks and Minor Mergers?

Itsuki Ogami [1,2,3] Sakurako Okamoto [4,5,1] Annette M.N. Ferguson [6] Yutaka Komiyama [3]
Masashi Chiba [7] Jin Koda [8] Kohei Hayashi [9,7,10] and Yoshihisa Suzuki [7]

[1] *National Astronomical Observatory of Japan, 2-21-1 Osawa, Mitaka, Tokyo 181-8588, Japan*
[2] *The Institute of Statistical Mathematics, 10-3 Midoricho, Tachikawa, Tokyo 190-8562, Japan*
[3] *Department of Advanced Sciences, Faculty of Science and Engineering, Hosei University, 3-7-2 Kajino-cho, Koganei, Tokyo 184-8584, Japan*
[4] *Subaru Telescope, National Astronomical Observatory of Japan, 650 North A'ohoku Place, Hilo, HI 96720, U.S.A.*
[5] *The Graduate University for Advanced Studies (SOKENDAI), 2-21-1 Osawa, Mitaka, Tokyo 181-8588, Japan*
[6] *Institute for Astronomy, University of Edinburgh, Royal Observatory, Blackford Hill, Edinburgh, EH9 3HJ U.K.*
[7] *Astronomical Institute, Tohoku University, Aoba-ku, Sendai, Miyagi 980-8578, Japan*
[8] *Department of Physics and Astronomy, Stony Brook University, Stony Brook, NY 11794-3800, U.S.A.*
[9] *National Institute of Technology, Sendai College, Sendai, Miyagi 989-3128, Japan*
[10] *Institute for Cosmic Ray Research, The University of Tokyo, Kashiwa, Chiba 277-8582, Japan*

ABSTRACT

We present the confirmation and characterization of a long stream (S-stream) in the southern part of M83. This feature is revealed using deep wide-field photometric data obtained by the Hyper Suprime-Cam (HSC) mounted on the Subaru Telescope. Using individual red giant branch (RGB) stars, we successfully trace the stream over a large length of ~ 81 kpc and a considerable width of ~ 9 kpc. With a mean surface brightness of $\langle \mu_V \rangle \sim 31.8^{+1.3}_{-1.9}$ mag arcsec^{-2}, it is one of the most diffuse extragalactic streams currently known. The mean photometric metallicity of the stream is $\langle [\mathrm{M/H}] \rangle = -1.23 \pm 0.02$ dex with a standard deviation of 0.28 ± 0.01 dex, and we estimate the stellar mass to be $(8.5^{+4.2}_{-2.8}) \times 10^6$ $\mathrm{M}_\odot$ from the luminosity of RGB stars. Compared to its well-known northern counterpart, the S-stream is slightly more metal-poor, but our large-area RGB map shows compelling evidence that these two features are related, originating from a single low-mass merger event. We identify density variations along the S-stream, which more likely reflect intrinsic density structure within the progenitor rather than the interaction with dark matter subhalos. Similarities between the morphology of the S-stream and some features in the H I distribution suggest that a minor merger event may have disturbed and redistributed M83's outer H I gas, leading to triggered star formation and the formation of the XUV disk.

M83=NGC 5236, Sc

H-alpha

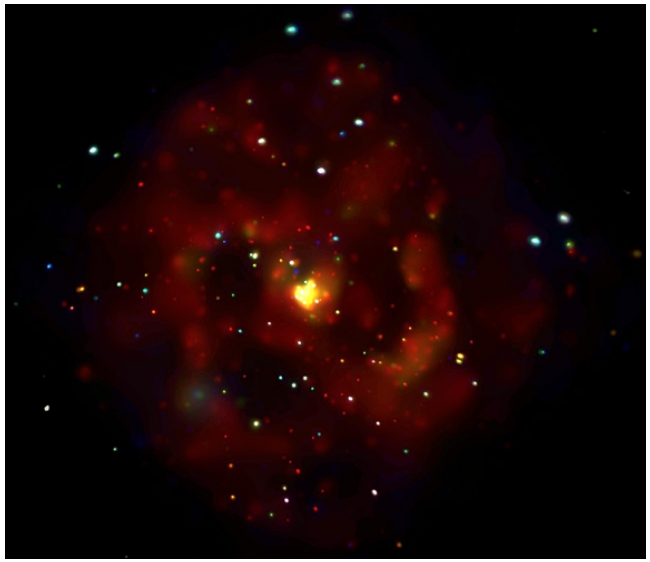

X-ray

UV

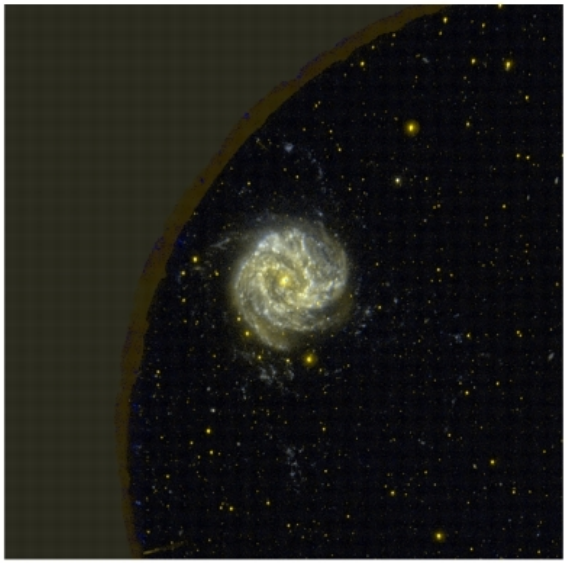

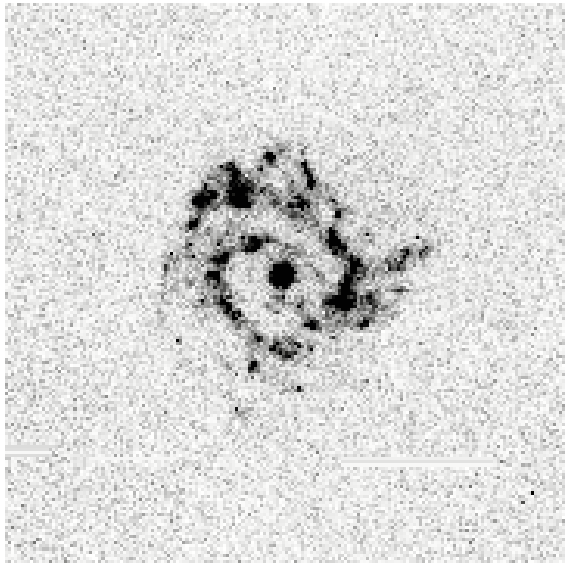

Потоки из красных гигантов

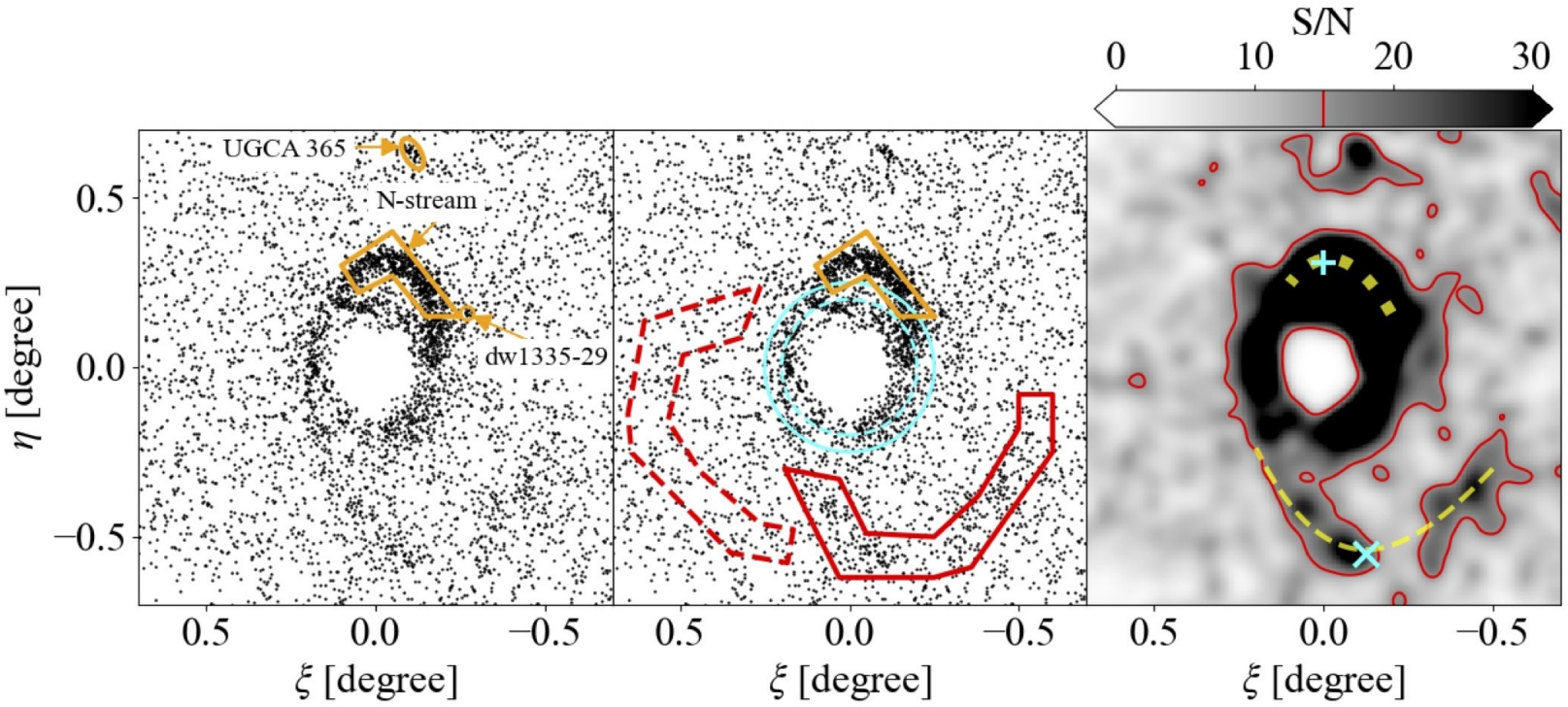

Figure 1. Left: The spatial distribution of RGB stars around M83. These stars are extracted from the CMD box defined by the solid red polygon in Figure 2. The known substructure and satellite galaxies are outlined in orange. Middle: The same as in the left panel, but with the solid red polygon indicating the recently-detected S-stream. The dashed red polygon shows the off-stream field, defined by rotating the solid red polygon 90 degrees clockwise around the center of M83. The cyan solid (dashed) circle indicates a region at 0.25 (0.20) degree from the center of M83. Right: the signal-to-noise ratio (S/N) map smoothed using a Gaussian kernel with a bandwidth of 1.2 arcmin. The red contour shows where the S/N reaches a value of 15. The yellow dashed and dotted lines represent the ridge lines of S-stream and N-stream, respectively. The cyan 'x'-mark ('+'-mark) corresponds to the densest parts of the S-stream (N-stream).

Характеристики потоков

Table 1. Photometric and structural properties of the M83 streams

Property	S-stream	N-stream
α	$13^{h}36^{m}25\overset{s}{.}65$	$13^{h}37^{m}01\overset{s}{.}50$
δ	$-30°25'03\overset{''}{.}76$	$-29°33'27\overset{''}{.}53$
projected separation [degree (kpc)]	0.57 (46)	0.23 (19)
width [degree (kpc)]	0.11 (9)	0.10 (8)
length [degree (kpc)]	0.99 (81)	0.40 (33)
M_V [mag]	$-10.72^{+0.54}_{-0.54}$ (a)	$-11.34^{+0.49}_{-0.49}$ (a)
M_i [mag]	$-11.66^{+0.06}_{-0.06}$ (a)	$-12.31^{+0.06}_{-0.06}$ (a)
$E(B-V)$ [mag]	0.05	0.04
$\langle(g-i)_0\rangle$ [mag]	$1.59^{+0.35}_{-0.35}$	$1.65^{+0.31}_{-0.31}$
$\langle$[M/H]$\rangle$ [dex]	$-1.23^{+0.02}_{-0.02}$	$-1.05^{+0.01}_{-0.01}$
$\sigma_{[M/H]}$ [dex]	$0.28^{+0.01}_{-0.01}$	$0.40^{+0.01}_{-0.01}$
$M_{*,flux}/M_\odot$	$(8.5^{+4.2}_{-2.8})\times10^6$ (b)	$(1.6^{+0.6}_{-0.5})\times10^7$ (b)
$M_{*,[Fe/H]}/M_\odot$ ([α/Fe] = 0.0)	$(3.4^{+3.8}_{-1.6})\times10^7$ (c)	$(13.6^{+15.5}_{-6.6})\times10^7$ (c)
$M_{*,[Fe/H]}/M_\odot$ ([α/Fe] = +0.2)	$(1.2^{+1.1}_{-0.5})\times10^7$ (c)	$(4.7^{+5.4}_{-3.6})\times10^7$ (c)
$\langle\mu_V\rangle$ [mag arcsec^{-2}]	$31.8^{+1.3}_{-1.9}$	$29.9^{+1.3}_{-2.1}$

NOTE—The equatorial coordinates indicate the southernmost position for the S-stream (cyan 'x'-mark in the right panel of Fig. 1) and the northmost position for the N-stream (cyan '+'-mark).

[a] V- and i-band absolute magnitudes are calculated under the assumption of the distance to M83.

[b] Estimated from the total flux within the solid red/orange box in the middle panel of Fig. 1.

[c] Estimated from the mass–metallicity relation assuming two α-enhancement cases ([α/Fe] = 0.0 and +0.2).

Характеристики звезд в потоках

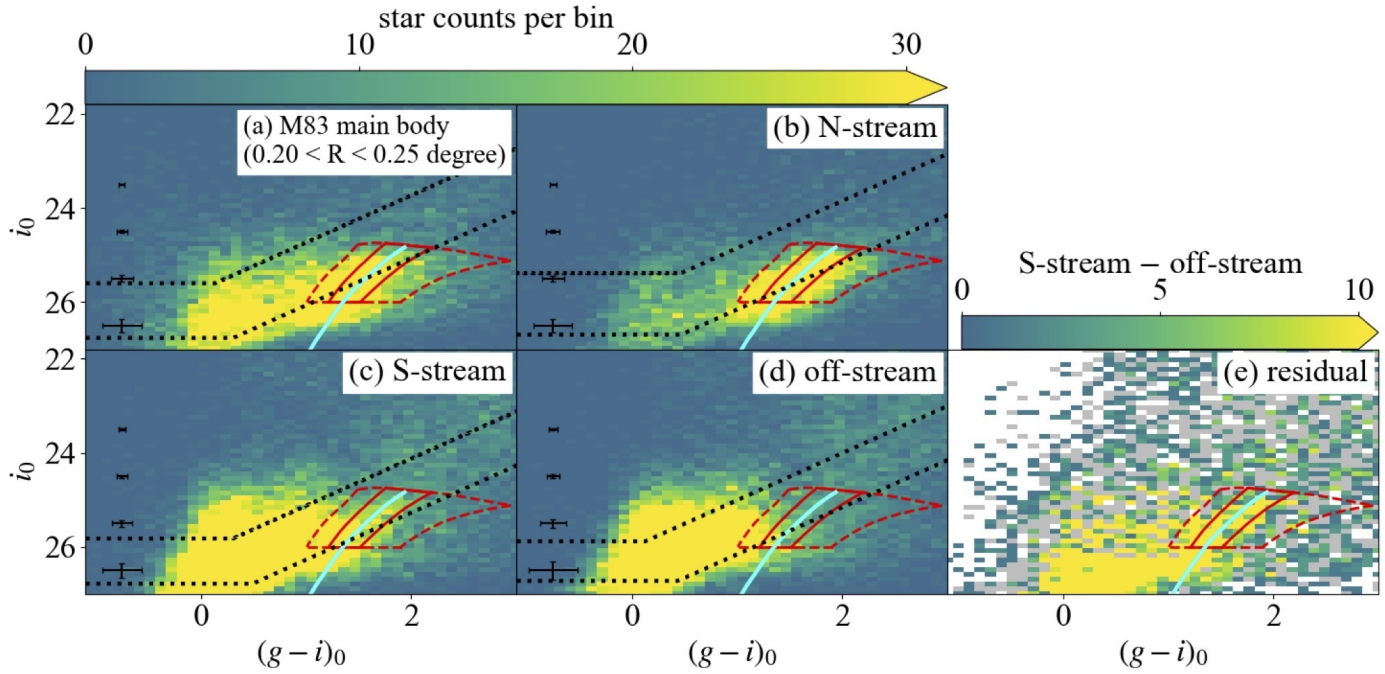

Figure 2. De-reddened Hess diagrams of the point sources in M83, the N-stream field, the S-stream field, the off-stream field, and the field-subtracted S-stream. The bin sizes are set to 0.1 mag along both the x- and y-axes. Panel (a): Stars located between 0.20 degree and 0.25 degree from the center of M83. The solid (dashed) red box indicates the narrow (wide) RGB box used to select M83 RGB stars. The cyan solid line indicates the PARSEC isochrone (Bressan et al. 2012) of age 10 Gyr and [M/H] = −1.23 shifted to M83's distance. This cyan line illustrates the mean photometric metallicity of the S-stream estimated in Section 4.2. Error bars show the median photometric uncertainties of observed sources for each region. The black dashed curves represent the detection completeness limits at the 50% and 20% levels. Panel (b), (c), (d): The same as in panel (a), but for the stars within the N-stream polygon, the S-stream polygon, and the off-stream field. Panel (e): The field-subtracted Hess diagram of the S-stream field, constructed by subtracting panel (d) from (c). Gray-colored bins show those in which the count has negative values

Низкая металличность, газ = разорванный карлик

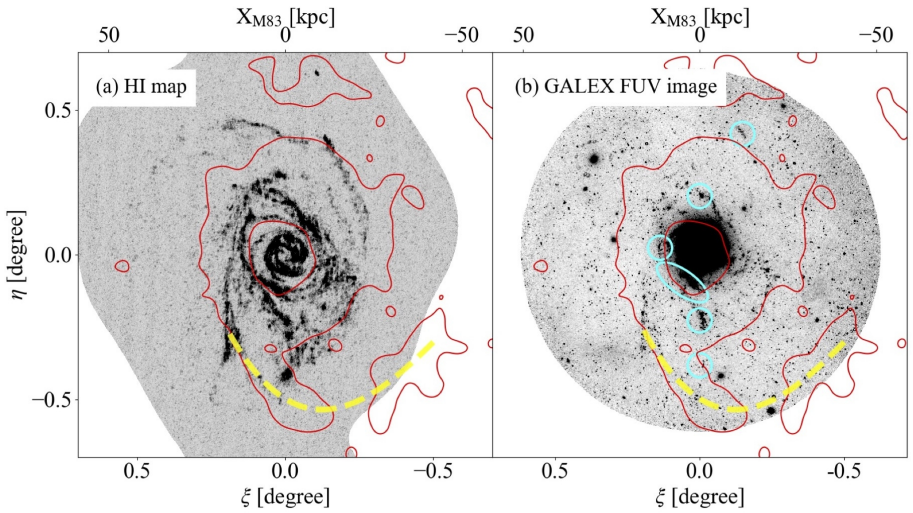

Figure 3. Panel (a): The H I map from Eibensteiner et al. (2023). The red contour shows the region within which the S/N of the binned smoothed RGB star-count map is ≥ 15 (see right panel of Figure 1), while the yellow dashed line represents the ridge line of the S-stream. Panel (b): The GALEX FUV image. Cyan circles and ellipses are regions that show peaks in the FUV emission defined by Eibensteiner et al. (2023). Red contour and yellow dashed line are the same as in Panel (a).

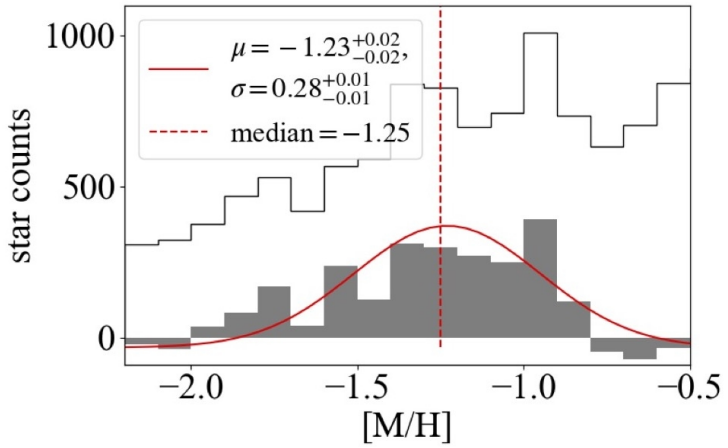

Figure 4. Completeness-corrected photometric metallicity distribution of RGB stars in the S-stream field. The open histogram shows the metallicity distribution of RGB stars, selected using the wide RGB-box, in the S-stream field, while the gray histogram shows the contaminant-subtracted metallicity distribution using the off-stream field. The solid red line shows a Gaussian fit to the contaminant-subtracted metallicity distribution, and the dashed red line illustrates the median value.

ArXiv: 2603.20360

GA-NIFS & JADES: Confirmation of pristine gas near GN-z11

H. Übler, R. Maiolino, P. G. Pérez-González, Y. Isobe, G. C. Jones, N. Kumari, S. Charlot, E. Rusta, et al.

(Full author list and affiliations details can be found after the references)

March 24, 2026

ABSTRACT

According to the leading cosmological model, a first generation of stars called Population III (PopIII), condensed almost entirely out of hydrogen and helium, must have initiated the creation of all heavier chemical elements. Here we report the detection of ionised hydrogen ($H\gamma_{4342}$) with S/N=5.9 in a region about 3 pkpc (projected) North-East from the z∼10.6 galaxy GN-z11, where line emission compatible with doubly ionised helium ($HeII_{1640}$) had been found. Our new *JWST*/NIRSpec-IFS G395H data confirm the authenticity of the previous detection, at a redshift of $z_{H\gamma}$=10.5862±0.0003. Hδ is marginally detected (S/N∼2). No metal lines are detected in our observations spanning λ_{rest}=0.25-0.45μm. We derive a 3σ upper limit on the gas phase metallicity of 12+log(O/H)<6.96 (Z_{gas}<0.019 $Z_{\odot}$). Through comparison with NIRCam imaging, we constrain a lower limit on the equivalent width of $EW_0(H\gamma)$>350Å. We compare our emission line constraints to model predictions and find them compatible with photoionization by PopIII stars, possibly intermixed with next-generation (PopII) stars. We infer an upper limit on the dynamical mass of $M_{dyn}\lesssim 3\times10^8 M_{\odot}$. Our data provide novel support for the presence of PopIII stars nearby GN-z11, 440 Myr after the Big Bang.

Эмиссионный спутник GN-z11

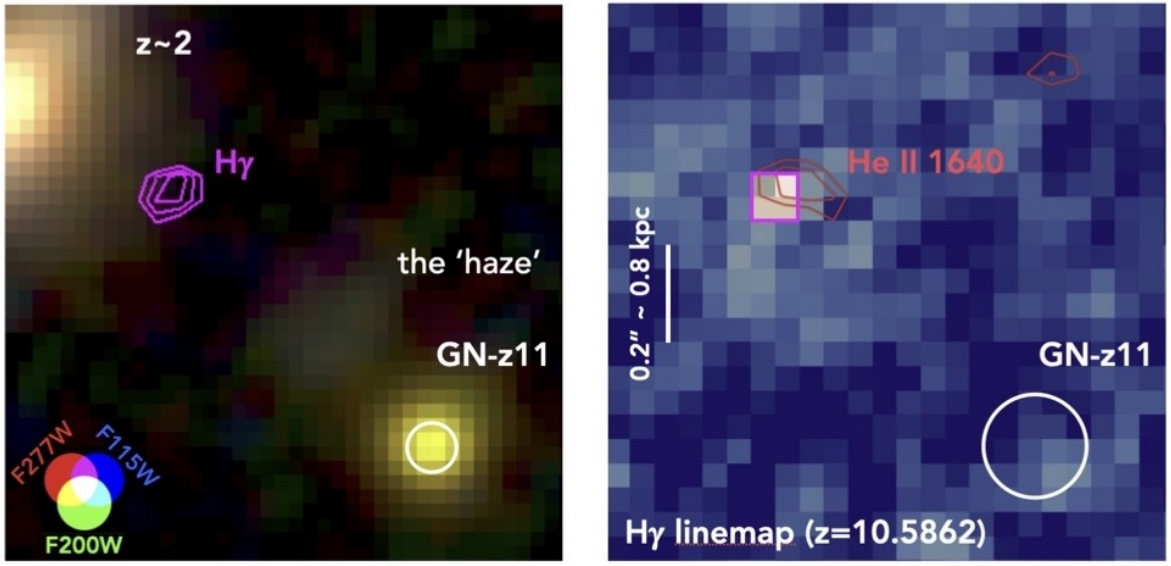

Fig. 1: *Left:* NIRCam *rgb* image showing the location of the Hγ clump (pink contours) in reference to GN-z11, the 'haze' (Tacchella et al. 2023), and a z~2 galaxy. The white circle indicates the astrometric uncertainty (r=0.05″) in registering the NIRCam images and NIRSpec-IFS cubes, comparable to the NIRCam PSF at 2.8μm (~0.09″). *Right:* Hγ linemap (λ_{obs}=5.029-5.031μm). The pink square shows the extraction aperture for Fig. 2. Red contours trace HeII$_{1640}$ by M26. The circle shows the NIRSpec PSF at 5.3μm.

Эмиссионные линии – только водородные

Table 1: R~2700 emission line fluxes from Gaussian fits and upper limits in units of 10^{-20} erg/s/cm^2, extracted from the integrated spectrum (Fig. 2). Flux uncertainties are calculated from the local noise. For non-detections, we calculate 3σ flux upper limits from 500 Monte Carlo realisations of the spectrum. The third column provides fluxes corrected for magnification by the foreground galaxy, and for aperture losses assuming a point-source geometry for the line-emitting region. The lower limit for $EW_0(H\gamma)$ is calculated by comparing the aperture-corrected flux to the 5σ upper limit continuum magnitude.

Line	Flux (0.1″×0.1″)	Flux (magn. & ap. corr.)
$H\gamma$	4.1 ± 0.7	16.0 ± 2.7
$H\delta$	1.2 ± 0.6	4.4 ± 2.2
$H\epsilon$	< 3.1	< 11.5
He I$_{3890}$	< 2.0	< 7.0
[OIII]$_{4364}$	< 3.8	< 14.9
[NeIII]$_{3870}$	< 1.8	< 6.3
[OII]$_{3730}$	< 2.1	< 7.4
[OII]$_{3727}$	< 2.5	< 8.8
$EW_0(H\gamma)$ [Å]	–	> 350

Вот так выглядит спектр

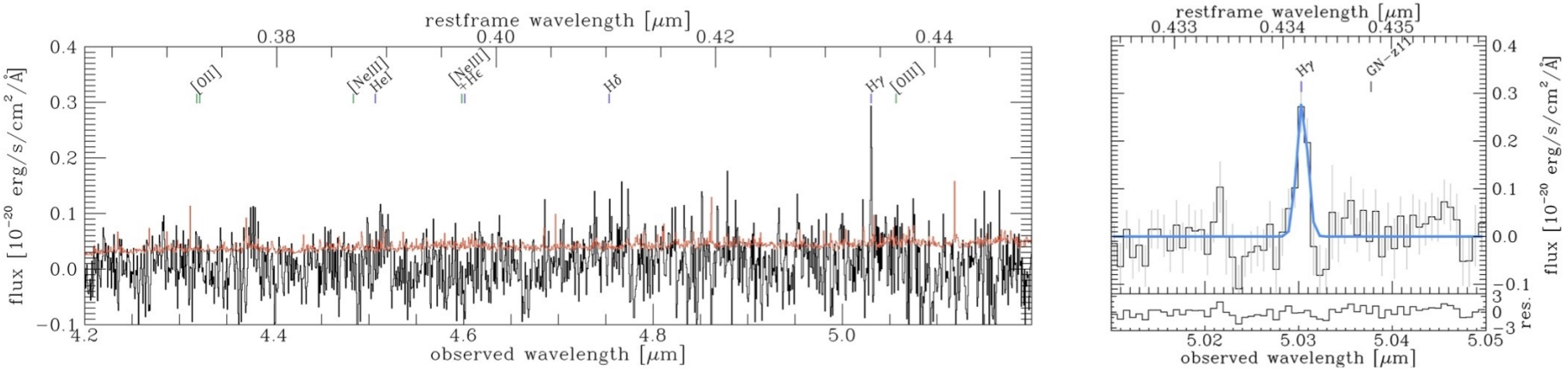

Fig. 2: *Left:* Integrated spectrum of the Hγ clump (pink aperture in Fig. 1). The error spectrum is shown in red. We indicate the theoretical locations of several emission lines at z=10.586. *Right:* Best fit to Hγ, detected with S/N~6. In grey we mark the wavelength of Hγ in GN-z11.

Population III?

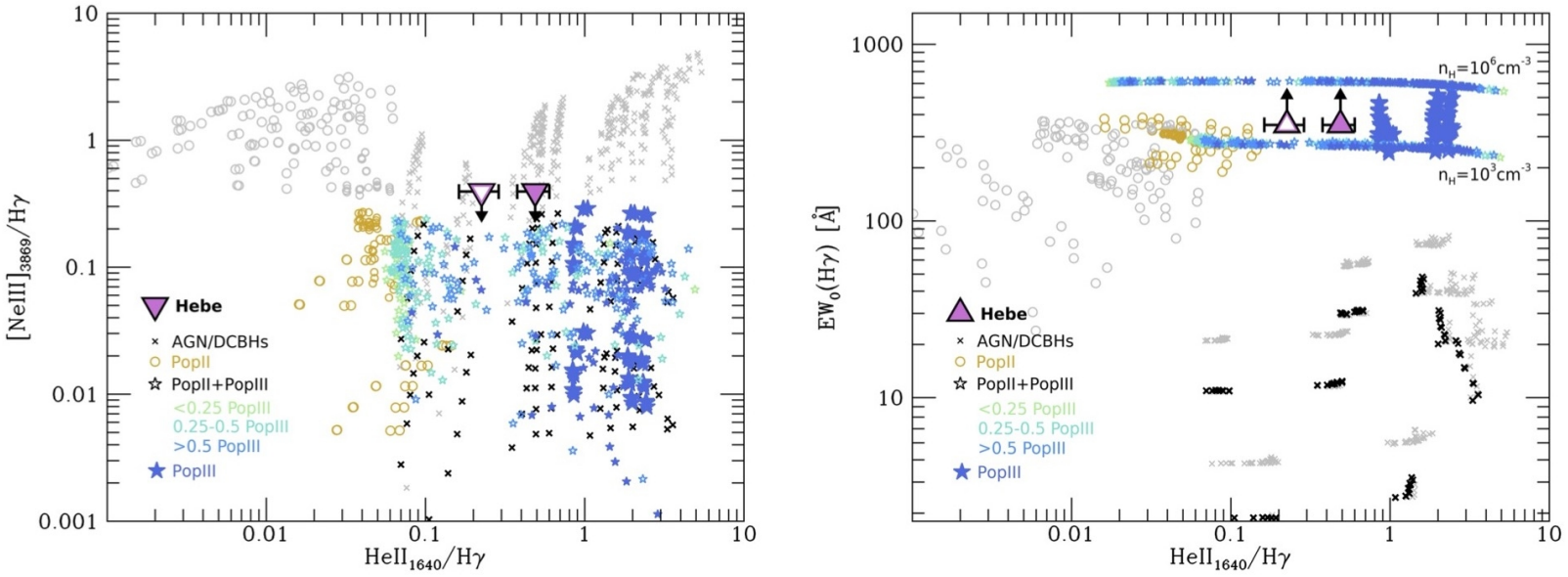

Fig. 3: Diagnostic diagrams of [Neiii]$_{3870}$/Hγ (*left*) and EW$_0$(Hγ) (*right*) *vs.* Heii$_{1640}$/Hγ. Pink triangles shows our constraints for Hebe from this work and M26, using either the total Heii flux (filled) or only the Heii component matching our Hγ detection (open; 'C2', see M26 and Appendix A). Other symbols show model predictions by Nakajima & Maiolino (2022) and Rusta et al. (2025) (small stars) for ionisation by PopIII (filled stars), mixed PopIII+PopII (open stars; fractions of total stellar mass), PopII (open circles) and AGN or DCBHs (crosses). For PopIII stars, the models shown have stellar masses $M_\star$=1-500$M_\odot$, absolute gas phase metallicity Z=0-10^{-4}, neutral hydrogen density n_H=10$^{3-6}$cm^{-3}, ionisation parameter log(U)=[−0.5; −2] for Nakajima & Maiolino (2022), and $M_\star$=0.8-1000$M_\odot$, Z=0-2.7×10^{-4}, n_H=10^{3}cm^{-3}, log(U)=−1 (and n_H=10^{6}cm^{-3}, log(U)=−2 in the right panel) for Rusta et al. (2025). Models with gas metallicities conflicting with our upper limit are greyed out. Our observational constraints are compatible with ionisation by (self-enriched) PopIII, or PopIII mixed with PopII.

ArXiv: 2603.20362

The search for Population III: Confirmation of a HeII emitter with no metal lines at z=10.6

Roberto Maiolino,[1,2,3] ⋆ Hannah Übler,[4] Michele Perna,[5] Joris Witstok,[6,7] Gareth C. Jones,[1,2] Pablo G. Pérez-González,[5] Kimihiko Nakajima,[8,9,10] Elka Rusta,[11,12] Stefania Salvadori,[11,12] Sandro Tacchella,[1,2] Piero Madau,[13,14] James A. A. Trussler,[15] Francesco D'Eugenio,[1,2] Xihan Ji,[1,2] Jan Scholtz,[1,2] Stefano Carniani,[16] Yuki Isobe,[1,2,17] Harley Katz,[18,19] Santiago Arribas,[5] William M. Baker,[20] Torsten Böker,[21] Volker Bromm,[22,23,24] Andrew J. Bunker,[25] Stephane Charlot,[26] Jacopo Chevallard,[25] Giovanni Cresci,[12] Mirko Curti,[27] Emma Curtis-Lake,[28] Daniel Eisenstein,[15] Eiichi Egami,[29] Andrea Ferrara,[16] Luca Graziani,[30,31] Kevin Hainline,[29] Jakob M. Helton,[32] Lucy R. Ivey,[1,2] Benjamin D. Johnson,[15] Ignas Juodžbalis,[1,2] Maria Koller,[1,2] Nimisha Kumari,[33] Nicolas Laporte,[34] Alessandro Marconi,[11,12] Giovanni Mazzolari,[4] Eleonora Parlanti,[16] Robert Pascalau,[1,2] Laura Pentericci,[35] Pierluigi Rinaldi,[36] Brant Robertson,[14] Bruno Rodríguez Del Pino,[5] Raffaella Schneider,[30] Alessandra Venditti,[22,24] Giacomo Venturi,[16] Christopher N. A. Willmer,[29] Callum Witten,[37] Sandra Zamora[16]

30 March 2026

ABSTRACT

We report the confirmation of a HeIIλ1640 emitter located at 3 pkpc from the galaxy GN-z11, at z=10.6. The detection, based on JWST NIRSpec-IFU high-resolution spectroscopy, confirms a previous claim based on medium-resolution spectroscopy. The HeIIλ1640 identification is further supported by the independent detection of Hγ obtained by Übler et al. (2026) at the same location. The HeII emission is spectrally resolved in two components separated by 120 km/s. The Equivalent Width of the HeII emission is extremely high (>20Å). No metal lines are detected. We argue that Population III stars are the most plausible explanation for the observed He II emission, with no satisfactory alternative from other classes of sources or mechanisms.

Эмиссионная линия гелия

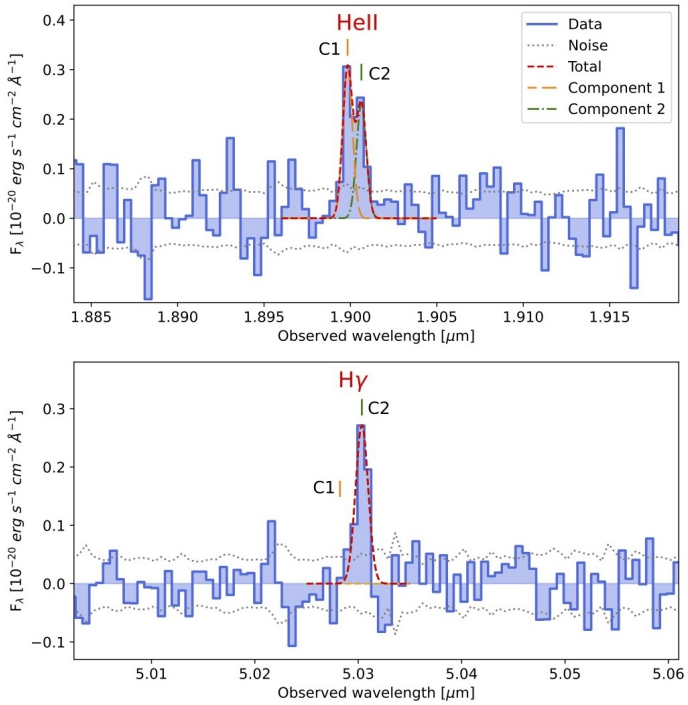

Figure 1. Top: *Hebe*'s spectrum around the wavelength of HeIIλ1640. Bottom: *Hebe*'s spectrum around Hγ, from Übler et al. (2026). The long-dashed (orange) and dot-dashed (green) lines show the simultaneous fit of HeII and Hγ with two components (C1 and C2), respectively, while the short-dashed red line shows the total; only C2 is detected in Hγ. The flux scale is not corrected for aperture losses nor for lensing magnification.

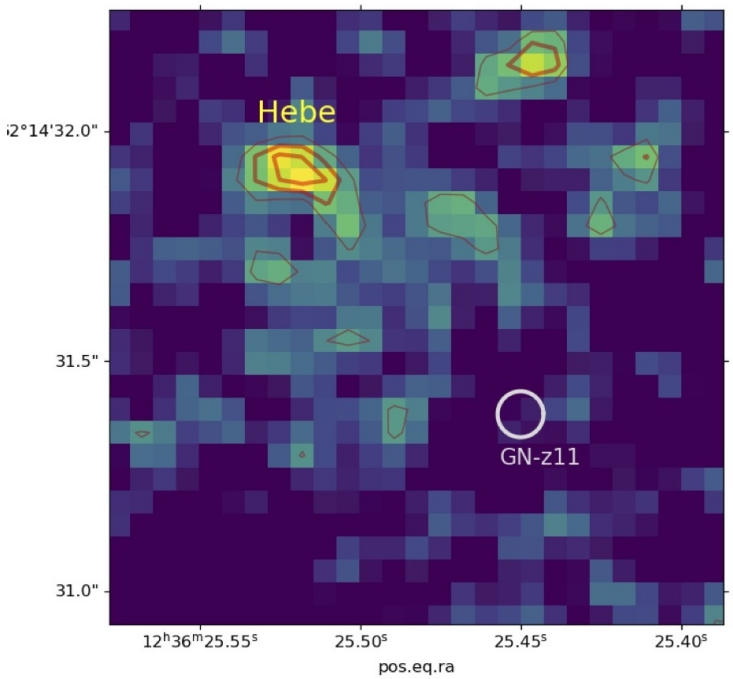

Figure 2. Continuum-subtracted map of the HeII emission at the redshift of *Hebe* in the halo of GN-z11 (see text). Contours indicate the 3σ (thin), 4σ and 5σ (thick) levels. The white circle indicates the location of GN-z11.

Полная карта

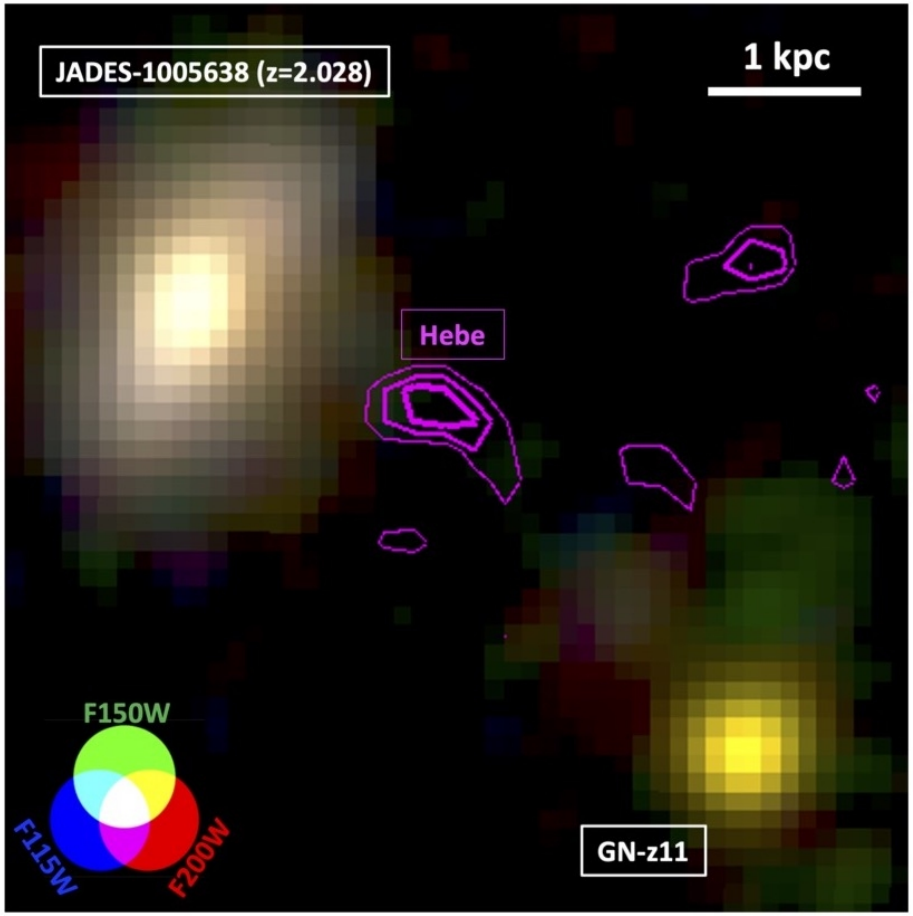

Figure 3. Same map of the HeII emission as in Fig.2 (contours), overlayed on the RGB image of the field from the NIRCam filters F115W, F150W and F200W, and with a 1.5″ × 1.5″ Field of View, adjusted to show the location of both GN-z11 and the foreground galaxy at z=2.03.

Верхние пределы на другие линии

Aperture corrected fluxes	
Total	
$F(HeII1640)$	$(1.11 \pm 0.17) \times 10^{-19}$ erg s^{-1} cm^{-2}
$EW_0(HeII1640)$	> 47Å
$NIV]_{1483,1486}/HeII$	$< 0.60^a$
$CIV_{1548,1551}/HeII$	$< 0.56^a$
$OIII]_{1661,1666}/HeII$	$< 0.63^a$
$NIII]_{1749}/HeII$	$< 0.46^a$
$CIII]_{906,1908}/HeII$	$< 0.36^a$
$F200W$	<3.1 (<2.7)^b nJy
Component 1	
$F(HeII1640)$	$(6.7 \pm 1.2) \times 10^{-20}$ erg s^{-1} cm^{-2}
$EW_0(HeII1640)$	> 28Å
Component 2	
$F(HeII1640)$	$(5.1 \pm 1.1) \times 10^{-20}$ erg s^{-1} cm^{-2}
$EW_0(HeII1640)$	> 22Å
De-lensed luminosities and cleaned of diffuse component	
$L(HeII1640)$ (total)	$(8.54 \pm 1.29) \times 10^{40}$ erg s^{-1}
$L(HeII1640)$ (C1)	$(5.1 \pm 0.9) \times 10^{40}$ erg s^{-1}
$L(HeII1640)$ (C2)	$(3.9 \pm 0.9) \times 10^{40}$ erg s^{-1}

Table 1. Fluxes and equivalent widths for *Hebe* and upper limits of the associated emission lines. The fluxes in the upper section are corrected for aperture losses. The luminosity in the bottom section are also corrected for a lensing magnification factor of 1.42 and also for the contribution of the diffuse component, as discussed in the text. Upper limits of all emission lines are at 3σ. Notes: ^{a}for all doublets/multiplets the table reports the upper limit on each individual component of the doublet, as they would be spectrally resolved; ^{b}the F200W upper limit is at 5σ, aperture-corrected for the NIRCam PSF – the value in parentheses is corrected for the HeII line contribution to F200W.

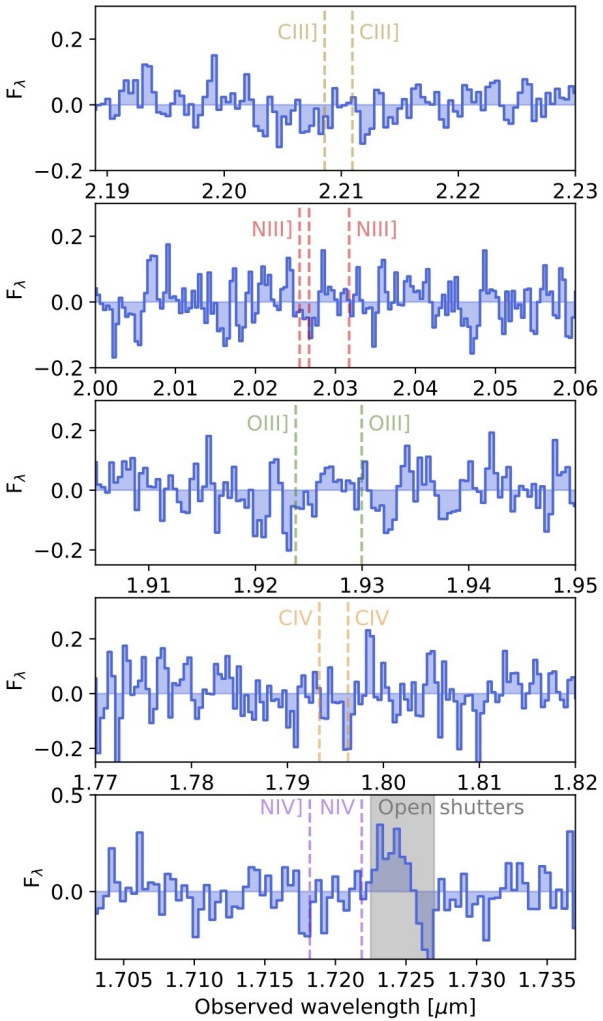

Figure B1. Spectrum of *Hebe* zoomed at the wavelengths where typically the strongest metal lines are observed in normal galaxies, specifically, from top to bottom: CIII]1906,1908, OIII]1661,1666, NIII]1749 multiplet, CIV1548,1551, and NIV]1483,1486. The gray shaded region in the bottom panel marks an unmasked faint open shutter/artefact affecting that spectral region. The units of the y axis are in 10^{-20} erg s^{-1} cm^{-2} Å^{-1}.

Население III?

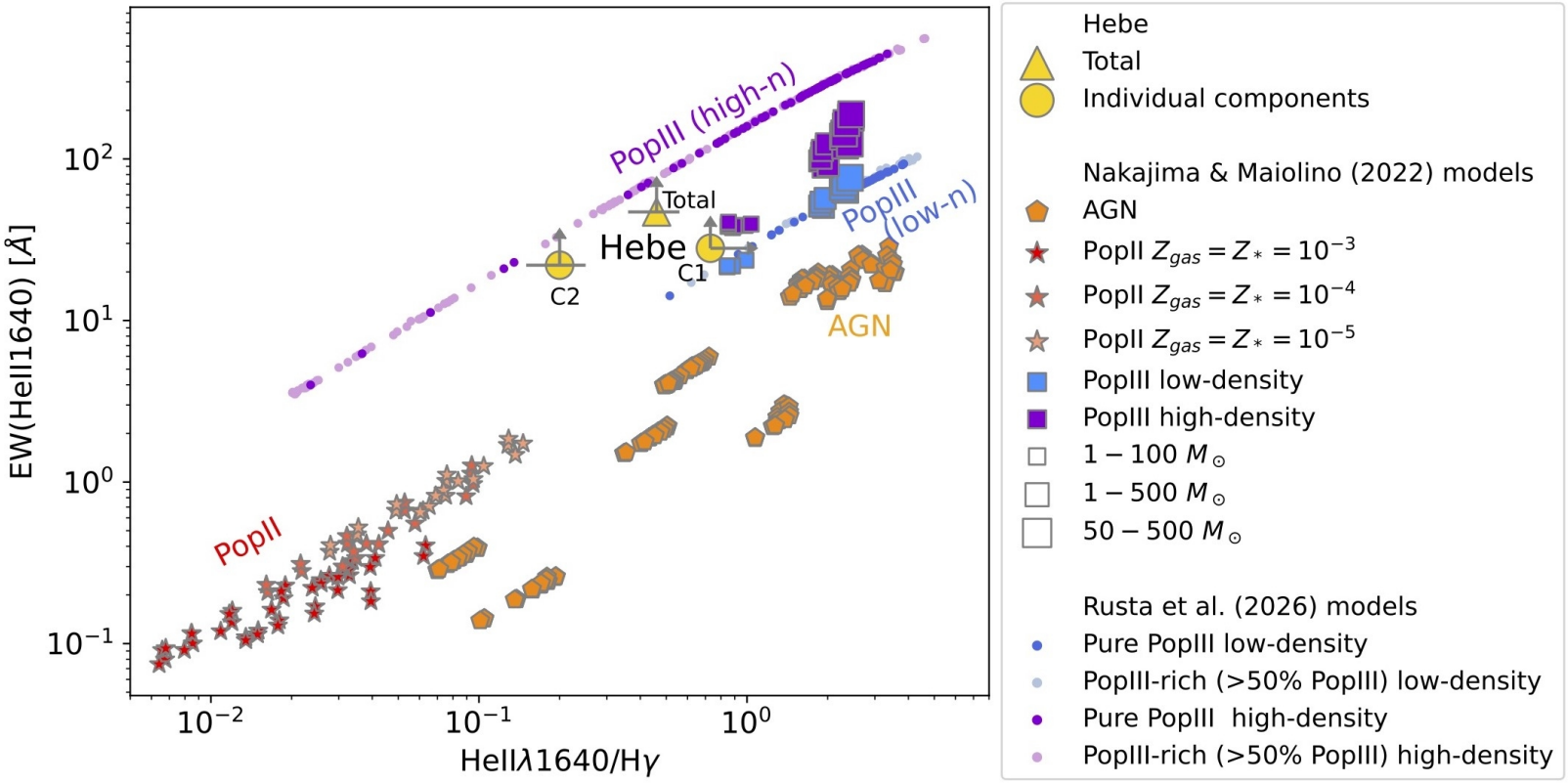

Figure 5. EW(HeII1640) versus HeII/Hγ diagnostic diagram. Various symbols show models from Nakajima & Maiolino (2022) for different classes of objects, specifically: squares - PopIII (blue: density $n = 10^3$ cm^{-3}; purple: densities $n = 10^5$ cm^{-3} and 10^6 cm^{-3}); red stars - PopII with decreasing metallicity, from darker to lighter, as indicated in the legend; orange pentagons - AGN. The sizes of the PopIII symbols reflect different IMFs. The small points are pristine PopIII models from Rusta et al. (2026), from pure PopIII (dark symbols) to cases with PopII contribution but still PopIII-dominated (PopIII >50% in mass, light symbols). The large golden symbols are the values inferred for *Hebe*, both the total and individual components, as indicated.

Альтернативные объяснения

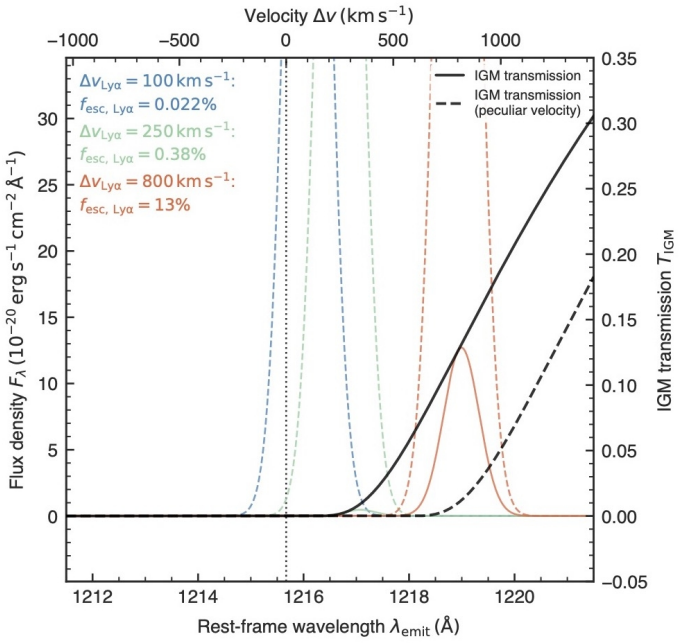

Figure 6. IGM transmission curve of a fully neutral IGM at $z = 10.586$ (solid black line). Dashed colored lines show model Lyα line profiles of *Hebe* assuming different velocity offsets from systemic, normalized to the case-B expectation based on the Hγ line strength. Transmitted profiles are shown by solid lines, although only the case of $\Delta v_{\mathrm{Ly}\alpha} = 800\,\mathrm{km/s}$ has sufficient transmission for it to be clearly visible. Also shown is the case where *Hebe* has a peculiar velocity of $-450\,\mathrm{km/s}$ relative to GN-z11 (dashed black line), which is expected to cause near-complete absorption of any Lyα emission.

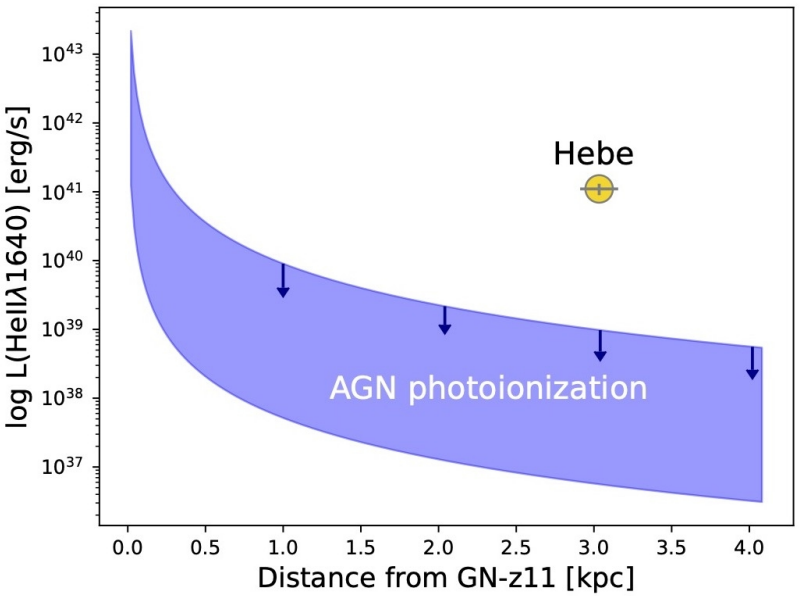

Figure 7. Expected maximum HeII luminosity resulting from a cloud photoionized by the AGN in GN-z11, as a function of distance from the latter. These are conservative upper limits, as it is assumed that the projected distance of the putative cloud from GN-z11 is the actual distance (in addition to other conservative assumptions discussed in the text). The golden circle shows the HeII luminosity of *Hebe* at the observed projected distance.